Coherent combining of high brightness tapered amplifiers for efficient non-linear conversion

Albrodt, P.; Jamal, Muhammad Tahir; Hansen, A. K.; Jensen, Ole Bjarlin; Blume, G.; Paschke, K.; Crump, P.; Georges, P.; Lucas-Leclin, G.

Published in:
Optics Express

Link to article, DOI:
10.1364/OE.27.000928

Publication date:
2019

Document Version
Publisher's PDF, also known as Version of record

Research Article | Vol. 27, No. 2 | 21 Jan 2019 | OPTICS EXPRESS 928
Optics EXPRESS

Coherent combining of high brightness tapered amplifiers for efficient non-linear conversion

P. ALBRODT,[1] M. T. JAMAL,[2] A. K. HANSEN,[2] O. B. JENSEN,[2] G. BLUME,[3] K. PASCHKE,[3] P. CRUMP,[3] P. GEORGES,[1] AND G. LUCAS-LECLIN[1,*]

[1]*Laboratoire Charles Fabry, Institut d'Optique Graduate School, CNRS, Université Paris Saclay 91127 Palaiseau Cedex, France*
[2]*DTU Fotonik, Department of Photonics Engineering, Technical University of Denmark, Frederiksborgvej 399 4000 Roskilde, Denmark*
[3]*Ferdinand-Braun-Institut, Leibniz-Institut für Höchstfrequenztechnik, Gustav-Kirchhoff-Str. 4 12489 Berlin, Germany*
**gaelle.lucas-leclin@institutoptique.fr*

Abstract: We report on a coherent beam combination of three high-brightness tapered amplifiers, which are seeded by a single-frequency laser at λ = 976 nm in a simple architecture with efficiently cooled emitters. The maximal combined power of 12.9 W is achieved at a combining efficiency of > 65%, which is limited by the amplifiers' intrinsic beam quality. The coherent combination cleans up the spatial profile, as the central lobe's power content increases by up to 86%. This high-brightness infrared beam is converted into the visible by second harmonic generation. This results in a high non-linear conversion efficiency of 4.5%/W and a maximum power over 2 W at 488 nm, which is limited by thermal effects in the periodically poled lithium niobate (PPLN).

1. Introduction

High-power high-brightness diode lasers are in strong demand for many applications and benefit from their efficiency, reliability and compactness [1]. However, the power limit of diode lasers is much lower in the visible spectral range than in the near infrared and not all wavelengths are directly accessible with diode lasers. Nonlinear frequency conversion, like second harmonic generation (SHG) is an important technology for the development of high power laser sources in the visible spectral range. Efficient SHG requires a good beam quality, a narrow spectral linewidth and a high input power [2]. High conversion efficiencies are commonly achieved with diode pumped solid state and fiber lasers [3,4], however diode laser based visible light sources have become increasingly attractive for biomedical applications [5] to fulfill the need for compact and efficient visible laser sources. Different high-brightness diode laser architectures are used for blue-green light generation [6]. Among those, tapered lasers (TPL) and tapered amplifiers (TPA) are the most promising architecture since they combine high power and acceptable beam quality in one device.

TPL and TPA devices consist of a single mode ridge waveguide (RW) followed by flared gain-guided amplifier section. Spectrally stabilized TPL are available in the visible (VIS) and near-infrared (NIR) spectral range and reach output powers up to 15 W per device [7] and can be converted to multiple watts of VIS light [8] by making use of a cascade of two SHG crystals [9,10]. Further power scaling can be achieved using an increased NIR pump laser power enabled by research on highly efficient high power diode lasers [11]. Power can also be scaled by beam combining techniques. Incoherent spectral beam combining of tapered diode lasers is a straightforward concept for this power scaling [12], however the ultimate limitation is the available output power per wavelength channel. Coherent beam combining

#349135 https://doi.org/10.1364/OE.27.000928
Journal © 2019 Received 29 Oct 2018; revised 12 Dec 2018; accepted 17 Dec 2018; published 11 Jan 2019

Optics EXPRESS

(CBC) of light from several devices is the only way to achieve much higher powers within a single beam that retains excellent spatial and spectral beam quality [13].

We describe in this paper the CBC of three high-brightness tapered amplifiers in a simple optical setup. Furthermore, we demonstrate the importance of CBC for the development of high power visible light sources by demonstrating a significant improvement of the achievable nonlinear conversion efficiency for single pass SHG in a bulk periodically poled lithium niobate (PPLN) crystal.

2. Coherent beam combining

CBC is the superposition of multiple laser beams by constructive interference. It requires a proper and stable phase relationship of the sampled gain medium. Different approaches have been demonstrated: active phase locking of amplifiers seeded by a single frequency laser split into several beams or passive phase locking of emitters in an extended cavity [14]. Impressive results for CBC using a limited number of high power fiber amplifiers (P > 100W per channel) show the potential of power scaling by CBC reaching kW level powers [15,16]. CBC with diode lasers and amplifiers is still limited to lower power levels but has been demonstrated in various configurations. CBC of arrays of diode lasers in an external cavity [17–19] has been demonstrated but did not lead to a significant increase of the available NIR power since the combined power was limited to a few watts. CBC in MOPA configuration has been demonstrated for larger arrays of amplifiers [20,21] and led to a significant increase of the available NIR power of diode laser architectures reaching about 40 W for CBC of 47 Slab Coupled Optical Waveguide Amplifiers (SCOWA) [22].

Our approach to make CBC of diode lasers more attractive for future applications is to make use of high-brightness tapered amplifiers in order to reach similar power levels but with a reduced number of elements. Tapered laser diodes are a promising building block for CBC architectures as they can deliver high power in a close to diffraction limited beam out of one monolithic device. However, one important drawback to tapered devices is the slightly degraded beam quality at high powers with about 70% power-content in the diffraction limited central lobe while the rest of the power is distributed in side lobes. TPAs are nevertheless our preferred choice for power scaling by CBC to simplify the optical setup by using only a limited number of high-power amplifiers. At the same time as demonstrated in this study, CBC is one way to reduce the relative power content in the side lobes since CBC with non-perfect Gaussian beams favors the diffraction-limited power content leading to an improved beam quality [23]. In our previous studies, an output power of 11.5 W was reached by CBC of a monolithically integrated array of five TPAs, but it was limited by thermal effects caused by emitter to emitter heating of the laser bar [24]. For this reason, we make use of separate individual amplifiers that can be efficiently cooled in order to be able to operate them at higher currents and achieve a higher combined power per element [25]. Additionally one can develop a simplified optical setup with standard optical elements, as splitting and combining the beam is simpler.

2.1 Experimental setup

We used 6 mm long TPAs mounted p-side up on CuW-heat spreaders and C-mounts. We made use of amplifiers identical to lasers previously described in [26] but with a 2 mm long RW instead of the internal grating. Two amplifiers had a 5 µm wide single-mode RW entry section and the third amplifier a 4.5 µm wide entry section, limited by the availability of the amplifiers. Currents in RW (I_{rw}) and tapered section (I_{tp}) can be controlled independently, allowing decoupled control of the phase (via I_{rw}) and the power (via I_{tp}) in each amplifier. The amplifiers are saturated for ridge currents I_{rw} > 300 mA. We use small variations of I_{rw} above this limit in order to control the phase with limited impact on the optical power. The maximum power extracted from the amplifiers reaches 6.5 W at 10 A and is limited by thermal rollover due to poor thermal resistance of the c-mount packaging. The power content

Optics EXPRESS

in the central lobe is >70%. A detailed analysis of the amplifiers used is given in [25] showing that the phase noise of the amplifier is dominated by low frequencies (f < 10 Hz).

The CBC interferometer used in this work is sketched in Fig. 1 and is based on three arms. The seed laser, a narrow linewidth DFB laser at 976 nm (P_{max} = 100 mW), was isolated by a double stage optical isolator with an isolation > 50 dB. The beam was split and recombined using non-polarizing 50:50 beam splitters (BS). The beam was coupled into the ridge waveguides (RW) using aspheric lenses (L_2: f = 8 mm, NA = 0.5) and recollimated in the fast axis (FA) by an aspheric lens (L_3: f = 2.75 mm, NA = 0.55) and in the slow axis by a cylindrical lens (L_4: f = 19 mm). We note that the injection powers into the amplifiers were slightly different due to the asymmetry of the setup and the used 50:50 beam splitter coatings. However, this did not affect the performance of the setup since the input powers into all amplifiers (P_{in} ≥10 mW) were high enough to saturate them. The beams of amplifiers A_1 and A_2 interfered on a 50:50 beam combiner (BS_1). The combined beam was then directed to the second 50:50 beam combiner (BS_2) where it interfered with the beam from A_3. One path at each element of combination, representing the combining losses B_1 and B_2, was absorbed by a beam block. We note that the use of two 50:50 beam combiners leads to unbalanced intensities on the second combiner resulting in minor losses smaller than 3% in the combining setup [24]. The power of the combined beam is measured by a fast photodiode and a control loop is used to maximize and stabilize the output power by active feedback on the ridge currents of A_2 and A_3 sequentially. We used a standard hill climbing algorithm for the phase control, which is characterized in details in [25].

The output of the CBC interferometer was used for single pass SHG, which will be described later in section 3.

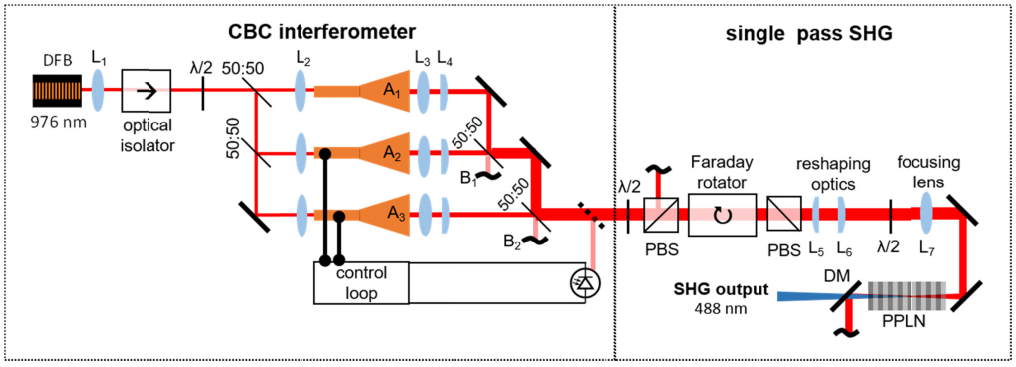

Fig. 1. Experimental setup of the CBC interferometer and the single pass SHG in a MgO:PPLN bulk crystal; BS: 50:50 beam splitters; PBS: polarizing beam splitters.

2.2 Combined power

We measured the coherently combined power P_{CBC} behind the combining elements at different currents into the tapered section, corresponding to the superposition of two and three beams, respectively (see Fig. 2). The positions of the cylindrical lenses for SA-collimation (Fig. 1) were adapted at each operating point to correct the astigmatism and to ensure a good beam overlap on the beam combiners. The combining efficiency is defined by the ratio of the coherently combined power over the sum of the extracted optical powers, which is equivalent to $\eta = P_{CBC} / (P_{CBC} + P_{B1} + P_{B2})$ for the superposition of A_{1+2+3} neglecting the losses at the optical elements. As shown in Fig. 2 we reached a maximum power of 12.9 W at I_{tp} = 10 A. This is higher than the 11.5 W previously achieved by CBC of 5 TPAs on a minibar limited by thermal effects [24]. Though the design of amplifiers in [24] was slightly different to those used in this work, it still appears that individual mounting of emitters allows the operation of the elements at higher currents since they can be cooled more efficiently.

Optics EXPRESS

Measurements of combination of only the first two amplifiers (A_{1+2}) show a higher combining efficiency (ranging from 85% at 2 A to 74% at 10 A). The combining efficiency of the total setup was > 65%. The combining efficiency decreases for higher currents in the tapered section caused by the degradation of the individual beam quality of each emitter, which will be discussed in the following subsection.

Measurements of the spectrum showed that the spectral properties of the DFB seed laser (976 nm) were maintained. The side mode suppression ratio was better than 40 dB. The full width at half maximum (FWHM) was smaller than 20 pm, limited by the resolution of the optical spectrum analyzer.

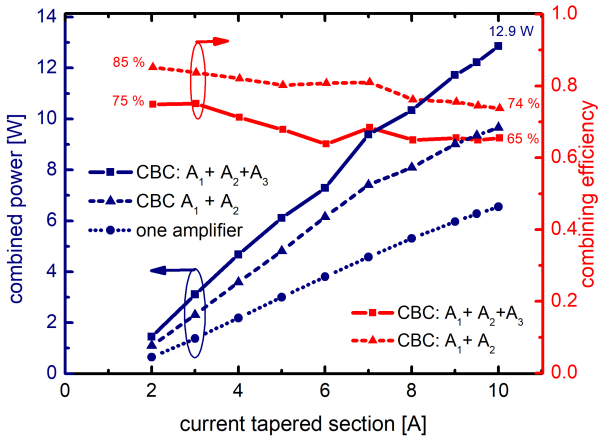

Fig. 2. Combined power at output and total combining efficiency as a function of the currents in the tapered section. The ridge currents were actively controlled in the range of 250 to 400 mA, the heatsink temperature was T = 20 °C. The astigmatism of the amplifiers was corrected at each operating current.

2.3 Beam quality and combining efficiency

Since the beam quality of the TPA is not diffraction limited in the slow axis (SA), one has to investigate the achievable combining efficiency together with the resulting beam quality of the combined beam. Two beams with a slightly different profile interfere at each combining element in the CBC interferometer (Fig. 1). The combining efficiency η at each combining step can be written as

$$\eta = \frac{\iint \eta'(x,y)\left[I_1(x,y)+I_2(x,y)\right]dxdy}{\iint I_1(x,y)+I_2(x,y)\,dxdy}, \tag{1}$$

with the local combining efficiency

$$\eta'(x,y) = \frac{1}{2}\frac{\left|\sqrt{I_1(x,y)}\,e^{i\varphi_1(x,y)}+\sqrt{I_2(x,y)}\,e^{i\varphi_2(x,y)}\right|^2}{\left|\sqrt{I_1(x,y)}\,e^{i\varphi_1(x,y)}\right|^2+\left|\sqrt{I_2(x,y)}\,e^{i\varphi_2(x,y)}\right|^2}, \tag{2}$$

defined by the overlap of the incident spatial amplitude and phase profiles $I_{1,2}(x,y)$ and $\varphi_{1,2}(x,y)$ respectively [27].

One can consider the beam of a tapered laser as a sum of the fundamental mode, corresponding to the central lobe, and emission at high angle ("side lobes"). The central lobes of each beam are very similar and interfere constructively with a high combining efficiency.

Optics EXPRESS

But the high-order modes exhibit a significantly higher beam mismatch and get therefore partially filtered during the CBC. Furthermore, amplified spontaneous emission is incoherent to the seed source and is therefore weakened by 50% at each beam combiner. Consequently, CBC of beams from tapered lasers leads to a clean-up of the spatial beam profile where the central lobe is maintained and the high angle non diffraction-limited emission is suppressed. The beam profile measurements shown in Figs. 3(a)-3(c) illustrate this effect. The shown beam profiles correspond to the beam waist after the focusing lens with a $1/e^2$ waist diameter of about 95 µm. One can clearly see that the side lobes in SA get filtered by the two CBC steps. The power content in the central lobe gets increased from 71% for one individual amplifier to 81% for CBC of A_{1+2} and 86% for CBC of A_{1+2+3}. As a result the beam quality factor is reduced from $M^2_{4\sigma} < 1.3 \times 4$ for one individual amplifier to $M^2_{4\sigma} < 1.1 \times 2.5$ for the final beam. Consequently the experimental combining efficiency of our setup is mostly limited by the power losses induced by this beam clean-up, which removes the undesired high-angle side lobes of the amplifier beams.

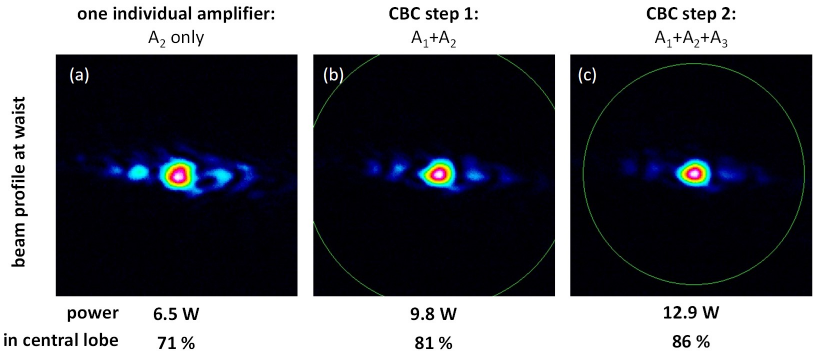

Fig. 3. Beam profiles at waist for (a) one individual amplifier A_2, (b) CBC of two amplifiers A_{1+2} and (c) the final CBC step of all three amplifiers A_{1+2+3}. Measurement for I_{tp} = 10 A, T = 20 °C and actively controlled ridge currents in the range of 250 to 400 mA. The FA is in vertical and the SA is in horizontal direction. The given central lobe power content was calculated by fitting a Gaussian beam profile to the central lobe of the beam and calculating the power content within the fitted profile.

In order to estimate the combining efficiency of the central lobes alone, we used intensity and wavefront measurements of the individual beams at maximum power. The combining efficiency is then calculated following Eqs. (1) and (2). We applied a strong clipping criterion at $1/e^2$ intensity level to the experimental data as a rough estimation for the central lobe and analyzed the overlap of the intensity and phase profiles within this area. We identified a mismatch of the intensity profile in SA caused by slightly different widths of the ridge section as mentioned earlier in section 2.1. Furthermore small differences in the collimation of each beam lead to a mismatch of the intensity profile in FA. Both effects reduce the achievable combining efficiency by 7-10% at each combining step. Furthermore, the wavefront measurements were used to evaluate combining losses linked to differences in the phase profile in between the beams. Those differences are small and had a limited impact smaller than 3% on the achievable combining efficiency of the central lobe.

Altogether, the calculated combining efficiency is η = 91% for the first CBC step (A_{1+2}) and η = 87% for the second step (A_{1+2+3}), resulting in an overall combining efficiency of 82% for the central lobe power content at the maximum current of 10 A. Our lower experimental combining efficiency of >65% considering the whole beam is thus clearly related to the power content in the fundamental mode of the individual amplifier beams.

Optics EXPRESS

3. Second harmonic generation

The increase of the brightness in the NIR by CBC of laser diodes can be useful for many applications requiring high power as well as good spectral and spatial beam quality. Especially for CW single-pass SHG, the conversion efficiency is strongly influenced by the focusing conditions in the nonlinear crystal, as described by Boyd and Kleinman [28]. Furthermore, the spatial quality of the pump beam directly impacts the achievable conversion efficiency [29]. We demonstrate in the following the improvement of single pass SHG efficiency resulting from the scaled brightness by coherent combining, and the subsequent increase of the visible power.

3.1 Description of the experiment

The output of the CBC-interferometer was used for single pass SHG as shown in Fig. 1. In order to test the nonlinear conversion efficiency at different levels of brightness, we did modify the CBC setup slightly in order to use the beam from either a single amplifier (A_1) or from the CBC of two (A_{1+2}) or three power amplifiers (A_{1+2+3}) as the input pump beam for the SHG. This was done by replacing the relevant combining elements with highly reflective mirrors. During the SHG experiments all three amplifiers were operated at constant current into the tapered section (I_{tp} = 9 A) and the power used for SHG was adjusted by turning the polarization before the first polarizing beam splitter (PBS). The optical isolation between the CBC interferometer and the SHG experiment was >25 dB. After reshaping optics (L_5: f = 50 mm and L_6: f = 100 mm) for beam size adjustment and astigmatism correction, another half-wave plate is used to align the polarization of the NIR beam with the crystallographic Z-axis of the nonlinear crystal which is parallel to the thickness of the crystal in this case. The NIR beam was then focused with a lens (L_7: f = 150 mm) into the 40 mm long periodically poled MgO:$LiNbO_3$ (PPLN). The $1/e^2$ waist diameter of the focused beam inside the crystal was measured to be ~95 µm, which was experimentally verified to be the optimum focusing condition at the highest input power. The focusing conditions were identical for all pump source configurations. The PPLN crystal was mounted into a temperature-controlled closed-top oven. The temperature was measured with a temperature sensor in the oven and corresponds to an average temperature. It was optimized at each pump power level. The spectral components were separated by a dichroic mirror (DM).

3.2 Experimental results

The SHG power was measured for three source configurations: a single amplifier (A_1), CBC of two amplifiers (A_{1+2}) and CBC of three amplifiers (A_{1+2+3}). Results are shown in Fig. 4. We fitted the pump depletion approximation [30]

$$P_{2\omega} = P_{\omega} \times \tanh^2(\sqrt{\eta P_{\omega}}), \tag{3}$$

where η is the nonlinear conversion efficiency, to the experimental values for pump powers < 6 W. The nonlinear conversion efficiencies in case A_1, A_{1+2} and A_{1+2+3} obtained by numerical fitting are 2.6%/W, 3.7%/W and 4.5%/W, respectively. This corresponds to an increase of up to 73% enhanced by the beam clean-up and the scaled brightness. We attribute the deviation of measured SHG power from the theoretical fit for $P_{\omega} \geq 6$ W to thermal dephasing due to localized heating caused by SH absorption [9]. This limited the maximum SHG output power to 2.09 W for 9.2 W of NIR input power (conversion efficiency >22%). However it is so far the highest power achieved at λ = 488 nm by single-pass SHG of a diode-laser-based system, thanks to the simultaneous increase of power and brightness provided by the coherent combining architecture.

Optics EXPRESS

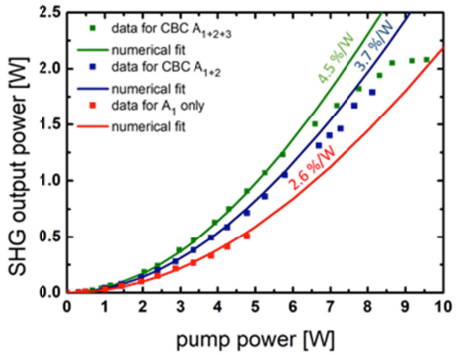

Fig. 4. SHG output power ($P_{2\omega}$) vs. fundamental pump power (P_{ω}) with corresponding numerical fits using pump depletion approximation.

A further investigation regarding the effects of thermal dephasing on the SHG power was performed by mechanical low frequency chopping (~0.7 Hz, 50% duty cycle) of the NIR beam at different pump power levels. Figure 5(a) shows a photodiode measurement of the SHG power and chopped pump beam with 7 W peak pump power. The results show a clear degradation in the SH power level during each pulse. This degradation in the SHG power indicates the onset of thermal dephasing. This effect was observed for pump powers higher than 6 W. The peak power of SHG can be considered as the SHG power level prior to adverse effects of thermal dephasing. When the peak power of SHG is plotted against the fundamental input power for $P_{\omega} > 6$ W, it followed the numerical fit nicely as shown in Fig. 5(b). This supports our conclusion that further increase of the SH power was limited by thermal effects in the PPLN crystal and not by the available pump power or the pump beam quality.

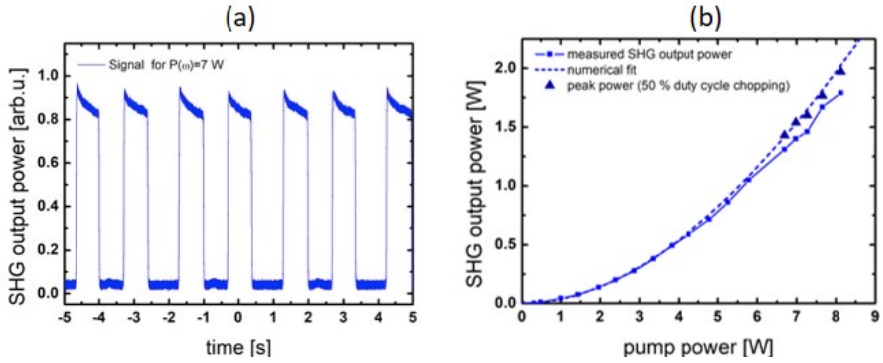

Fig. 5. (a) Photodiode measurements of the SHG output power with chopped pump beam. (b) SHG output power in CW and SHG peak power in QCW (50% duty cycle) operation. The used pump beam was generated by CBC of A_{1+2}.

The crystal temperature acceptance bandwidth measured at $P_{\omega} = 1$ W (blue curve) and $P_{\omega} = 7$ W (red curve) is shown in Fig. 6. The FWHM temperature bandwidth was about 0.6°C. The down shift of 0.4°C in the crystal phase matching temperature also indicates the overheating of the crystal due to SH absorption at high pump powers [4]. These thermal effects can be reduced by using nonlinear crystals with better thermal handling in a cascade scheme as described in [9,10].

Optics EXPRESS

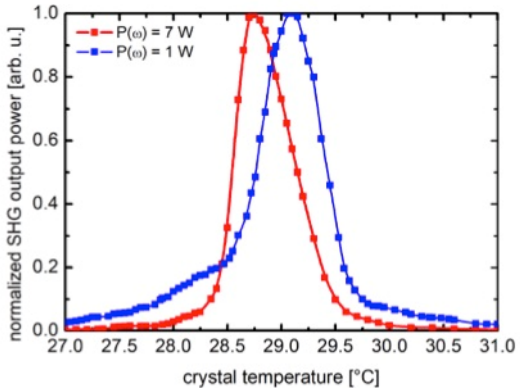

Fig. 6. Normalized SHG power vs. crystal temperature at P_ω = 1 W (blue curve) and P_ω = 7 W (red curve) under CW operation.

The measured spectral FWHM linewidth of the generated blue-green light (488 nm) was less than 20 pm limited by the resolution of the optical spectrum analyzer. The beam quality of SHG was close to diffraction-limited ($M_{4\sigma}^2 < 1.2$). The improved beam quality of the SHG beam compared to the fundamental input beam ($M_{4\sigma}^2 < 2.5$) is caused by the so-called nonlinear beam clean-up [31].

4. Conclusion and perspectives

Coherent beam combining is an important approach for power scaling of diode laser systems when high spatial quality and narrow linewidth are required. In this work, we used a simple architecture and only three amplifiers allowing to combine 12.9 W in one single beam. The beam quality was significantly increased by a beam cleanup inherent to the CBC process, resulting in a beam quality factor of $M_{4\sigma}^2 < 1.1 \times 2.5$ and 86% power content in the central lobe. Those results compare favorably with previous demonstrations of CBC with diode lasers [17–24], regarding both the combined power per amplifier and the simplicity of the setup. Furthermore, the multi-arm MOPA configuration used here could easily be scaled to a larger number of amplifiers, should a larger NIR power be required.

The coherently combined beam was used for single pass nonlinear frequency conversion in a PPLN crystal. As compared to direct SHG of single tapered devices, the improved beam quality of the combined beam in the infrared increases significantly the nonlinear conversion efficiency. A maximum SH power of 2.09 W at 488 nm was reached, limited by thermal dephasing of the PPLN, as confirmed using a pulsed pump beam. Further increase of the output power in the visible spectral range would firstly require the use of different nonlinear crystals in order to deal with the thermal roll-over of the conversion efficiency.

The CBC architecture demonstrated here relies only on off-the-shelf optical elements combined with state of art TPAs. As tapered amplifiers are now available at a wide range of wavelengths, from to the red to the NIR [7], our setup can easily be adapted for other applications. Besides its use for nonlinear frequency conversion towards the visible, our approach would also be effective to develop powerful pump sources for high-brightness pumping of fibre or bulk-crystal amplifiers. The output power could even be further increased by dense spectral beam combining of several similar CBC interferometers operating at slightly different wavelengths, as commonly used with single emitters and bars [32] offering a potential path to future CBC-based direct diode high brightness material processing systems.

Optics EXPRESS

Funding

European Union's Horizon 2020 research and innovation program under the Marie Skłodowska-Curie grant agreement No 721766.

Acknowledgment

Portions of this work were presented at the 8th EPS-QEOD Europhoton conference in 2018, TuM1.4. The authors are grateful to F. Moron for technical assistance.

References

1. F. Bachmann, P. Loosen, and R. Poprawe, *High Power Diode Lasers: Technology and Applications* (Springer Series in Optical Sciences, 2007).
2. R. W. Boyd, *Nonlinear Optics* (Elsevier, 2003).
3. G. D. Miller, R. G. Batchko, W. M. Tulloch, D. R. Weise, M. M. Fejer, and R. L. Byer, "42%-efficient single-pass cw second-harmonic generation in periodically poled lithium niobate," Opt. Lett. **22**(24), 1834–1836 (1997).
4. S. C. Kumar, G. K. Samanta, and M. Ebrahim-Zadeh, "High-power, single-frequency, continuous-wave second-harmonic-generation of ytterbium fiber laser in PPKTP and MgO:sPPLT," Opt. Express **17**(16), 13711–13726 (2009).
5. A. Müller, S. Marschall, O. B. Jensen, J. Fricke, H. Wenzel, B. Sumpf, and P. E. Andersen, "Diode laser based light sources for biomedical applications," Laser Photonics Rev. **7**(5), 605–627 (2013).
6. A. Jechow, R. Menzel, K. Paschke, and G. Erbert, "Blue-green light generation using high brilliance edge emitting diode lasers," Laser Photonics Rev. **4**(5), 633–655 (2010).
7. B. Sumpf and K. Paschke, "Spectrally stabilized high-power high-brightness DBR-tapered lasers in the VIS and NIR range," Proc. SPIE **10518**, 44 (2018).
8. O. B. Jensen, A. K. Hansen, A. Müller, B. Sumpf, P. M. Petersen, and P. E. Andersen, "Efficient generation of 3.5W laser light at 515nm by frequency doubling a single-frequency high power DBR tapered diode laser," Opt. Commun. **392**, 167–170 (2017).
9. A. K. Hansen, M. Tawfieq, O. B. Jensen, P. E. Andersen, B. Sumpf, G. Erbert, and P. M. Petersen, "Concept for power scaling second harmonic generation using a cascade of nonlinear crystals," Opt. Express **23**(12), 15921–15934 (2015).
10. S. C. Kumar, G. K. Samanta, K. Devi, and M. Ebrahim-Zadeh, "High-efficiency, multicrystal, single-pass, continuous-wave second harmonic generation," Opt. Express **19**(12), 11152–11169 (2011).
11. P. Crump, G. Erbert, H. Wenzel, C. Frevert, C. M. Schultz, K.-H. Hasler, R. Staske, B. Sumpf, A. Maassdorf, F. Bugge, S. Knigge, and G. Trankle, "Efficient High-Power Laser Diodes," IEEE J. Sel. Top. Quantum Electron. **19**(4), 1501211 (2013).
12. O. B. Jensen, A. K. Hansen, A. Muller, B. Sumpf, A. Unterhuber, W. Drexler, P. M. Petersen, and P. E. Andersen, "Power Scaling of Nonlinear Frequency Converted Tapered Diode Lasers for Biophotonics," IEEE J. Sel. Top. Quantum Electron. **20**(2), 307–321 (2014).
13. T. Y. Fan, "Laser beam combining for high-power, high-radiance sources," IEEE J. Sel. Top. Quantum Electron. **11**(3), 567–577 (2005).
14. G. D. Goodno and J. E. Rothenberg, "Engineering of Coherently Combined, High-Power Laser Systems," in *Coherent Laser Beam Combining* (Wiley-Blackwell, 2013), pp. 1–44.
15. A. Klenke, M. Müller, H. Stark, M. Kienel, C. Jauregui, A. Tünnermann, and J. Limpert, "Coherent Beam Combination of Ultrafast Fiber Lasers," IEEE J. Sel. Top. Quantum Electron. **24**(5), 1–9 (2018).
16. S. M. Redmond, D. J. Ripin, C. X. Yu, S. J. Augst, T. Y. Fan, P. A. Thielen, J. E. Rothenberg, and G. D. Goodno, "Diffractive coherent combining of a 2.5 kW fiber laser array into a 1.9 kW Gaussian beam," Opt. Lett. **37**(14), 2832–2834 (2012).
17. R. K. Huang, B. Chann, L. J. Missaggia, S. J. Augst, M. K. Connors, G. W. Turner, A. Sanchez-Rubio, J. P. Donnelly, J. L. Hostetler, C. Miester, and F. Dorsch, "Coherent combination of slab-coupled optical waveguide lasers," Proc. SPIE **7230**, 72301G (2009).
18. J. Montoya, S. J. Augst, K. Creedon, J. Kansky, T. Y. Fan, and A. Sanchez-Rubio, "External cavity beam combining of 21 semiconductor lasers using SPGD," Appl. Opt. **51**(11), 1724–1728 (2012).
19. B. Liu and Y. Braiman, "Coherent addition of high power broad-area laser diodes with a compact VBG V-shaped external Talbot cavity," Opt. Commun. **414**, 202–206 (2018).
20. S. M. Redmond, K. J. Creedon, J. E. Kansky, S. J. Augst, L. J. Missaggia, M. K. Connors, R. K. Huang, B. Chann, T. Y. Fan, G. W. Turner, and A. Sanchez-Rubio, "Active coherent beam combining of diode lasers," Opt. Lett. **36**(6), 999–1001 (2011).
21. J. L. Levy and K. Roh, "Coherent array of 900 semiconductor laser amplifiers," Proc. SPIE **2382**, 58–70 (1995).
22. K. J. Creedon, S. M. Redmond, G. M. Smith, L. J. Missaggia, M. K. Connors, J. E. Kansky, T. Y. Fan, G. W. Turner, and A. Sanchez-Rubio, "High efficiency coherent beam combining of semiconductor optical amplifiers," Opt. Lett. **37**(23), 5006–5008 (2012).

Optics EXPRESS

23. G. Schimmel, I. Doyen-Moldovan, S. Janicot, M. Hanna, J. Decker, P. Crump, G. Blume, G. Erbert, P. Georges, and G. Lucas-Leclin, "Rear-side resonator architecture for the passive coherent combining of high-brightness laser diodes," Opt. Lett. **41**(5), 950–953 (2016).
24. G. Schimmel, S. Janicot, M. Hanna, J. Decker, P. Crump, G. Erbert, U. Witte, M. Traub, P. Geaorges, and G. Lucals-Leclin, "Coherent beam combining architectures for high power tapered laser arrays," Proc. SPIE **10084**, 1008600 (2017).
25. P. Albrodt, M. Hanna, F. Moron, J. Decker, M. Winterfeldt, G. Blume, G. Erbert, P. Crump, P. Georges, and G. Lucas-Leclin, "Coherent combining of high brightness tapered lasers in master oscillator power amplifier configuration," Proc. SPIE **10514**, 105140T (2018).
26. C. Fiebig, G. Blume, C. Kaspari, D. Feise, J. Fricke, M. Matalla, W. John, H. Wenzel, K. Paschke, and G. Erbert, "12 W high-brightness single-frequency DBR tapered diode laser," Electron. Lett. **44**(21), 1253–1255 (2008).
27. G. D. Goodno, C.-C. Shih, and J. E. Rothenberg, "Perturbative analysis of coherent combining efficiency with mismatched lasers," Opt. Express **18**(24), 25403–25414 (2010).
28. G. D. Boyd and D. A. Kleinman, "Parametric interaction of focused Gaussian light beams," J. Appl. Phys. **39**(8), 3597–3639 (1968).
29. M. Uebernickel, R. Güther, G. Blume, C. Fiebig, K. Paschke, and G. Erbert, "Study of the properties of the SHG with diode lasers," Appl. Phys. B **99**(3), 457–464 (2010).
30. W. P. Risk, *Compact Blue-Green Lasers* (Cambridge University, 2003)
31. E. Karamehmedović, C. Pedersen, O. B. Jensen, and P. Tidemand-Lichtenberg, "Nonlinear beam clean-up using resonantly enhanced sum-frequency mixing," Appl. Phys. B **96**(2-3), 409–413 (2009).
32. U. Witte, F. Schneider, M. Traub, D. Hoffmann, S. Drovs, T. Brand, and A. Unger, "kW-class direct diode laser for sheet metal cutting based on DWDM of pump modules by use of ultra-steep dielectric filters," Opt. Express **24**(20), 22917–22929 (2016).